Crystallization of metastable phases and superconductivity in amorphous gallium antimonide

S. V. Demishev, Yu. V. Kosichkin, N. E. Sluchanko, and M. S. Sharambeyan

Institute of General Physics, Russian Academy of Sciences

A. G. Lyapin

Institute of High Pressure Physics, Russian Academy of Sciences

Structural relaxation and the crystallization of metastable phases have been studied in samples of amorphous gallium antimonide, a-GaSb, produced by quenching under pressure. The samples were studied by measurements of the temperature and time dependence of the resistivity, by differential thermal analysis, and by x-ray diffraction. A nonstoichiometric amorphous phase Ga_xSb_{1-x}, which arises in the interior of the sample under certain synthesis conditions, plays an important role in the relaxation and crystallization. The Ga_xSb_{1-x} phase with $x > 0.5$ causes a-GaSb superconductivity induced by the conversion to an amorphous state. The sequence of phase transitions and the resultant changes in the structure of the samples in the course of crystallization have been determined. As the temperature is raised to $T \sim 350$ K, a precrystallization process occurs in a-GaSb. This process consists of a decrease in the residual content of crystalline phase and a decrease in the maximum value of x in Ga_xSb_{1-x}, from $x \sim 1$ to $x \sim 0.8$, in the superconducting inclusions. At a higher temperature, $T \sim 350$–370 K, a Ga_xSb_{1-x} phase with $x \sim 0.8$ crystallizes. In the temperature range $T \sim 380$–500 K a tetrahedral amorphous phase of a-GaSb with $E_a = 1.4$ eV is observed to crystallize. In the same temperature range, at $T \sim 380$–430 K, the structure of the Ga_xSb_{1-x} inclusions with $x < 0.8$ changes, and these inclusions undergo a partial crystallization. As the annealing temperature is raised further, the superconductivity of the inclusions of the Ga_xSb_{1-x} phase is completely suppressed. The heat of crystallization of a-GaSb is 12–16 kJ/mole. There is a relationship between the deviation from stoichiometry, x, and the physical properties of the Ga_xSb_{1-x} phase, namely the crystallization temperature, the superconducting transition temperature T_c, and the upper critical field H_{c2}. The superconducting properties of the inclusions with $x < 0.8$ and $x > 0.8$ are quite different, possibly because of a change in the short-range order as x is varied. A general mechanism for the onset of superconductivity in two-component semiconductor systems is proposed. The applicability of this mechanism to epitaxial GaAs films is discussed. A method for structural analysis of the mixture of amorphous and crystalline phases which arises in the course of structural relaxation and crystallization is discussed. In this method it is possible to analyze the interface between the amorphous and crystalline regions. All phase-transition processes in a-GaSb are accompanied by changes in the structure of the boundary region.

1. INTRODUCTION

High-pressure synthesis (at $p \simeq 100$ kbar) has proved to be one of the most effective methods for putting III-V semiconductor compounds and also ZnSb, CdSb, etc., in an amorphous state.[1-3] A characteristic particularity of all these materials is a structural relaxation at temperature $T \leqslant T_{cr}$, where T_{cr} is the crystallization temperature.[4] According to the present understanding, this relaxation consists of an annealing of "defects" out of the amorphous network.

In compounds whose unit cell contains atoms of two or more species, e.g., GaSb, there is the possibility that structural defects will form upon the conversion to an amorphous state, because of a deviation from the stoichiometry of the original material. Furthermore, when an amorphous state is reached by way of a high-pressure crystalline phase of the original compound,[1-3] one might expect that structural defects would also be generated because the short-range order of the high-pressure phase would persist locally in several regions of the sample (the high-pressure phase is usually a lower-symmetry metallic phase characterized by a large coordination number).

Defects of this sort are of particular interest for bulk samples of amorphous gallium antimonide synthesized by quenching under pressure, because superconductivity is induced by the conversion to an amorphous state.[5,6]

It was shown in Refs. 5 and 6 that a-GaSb samples can be classified as either insulating or metallic on the basis of their conductivity, which depends on the conditions of their synthesis under a pressure of 90 kbar.
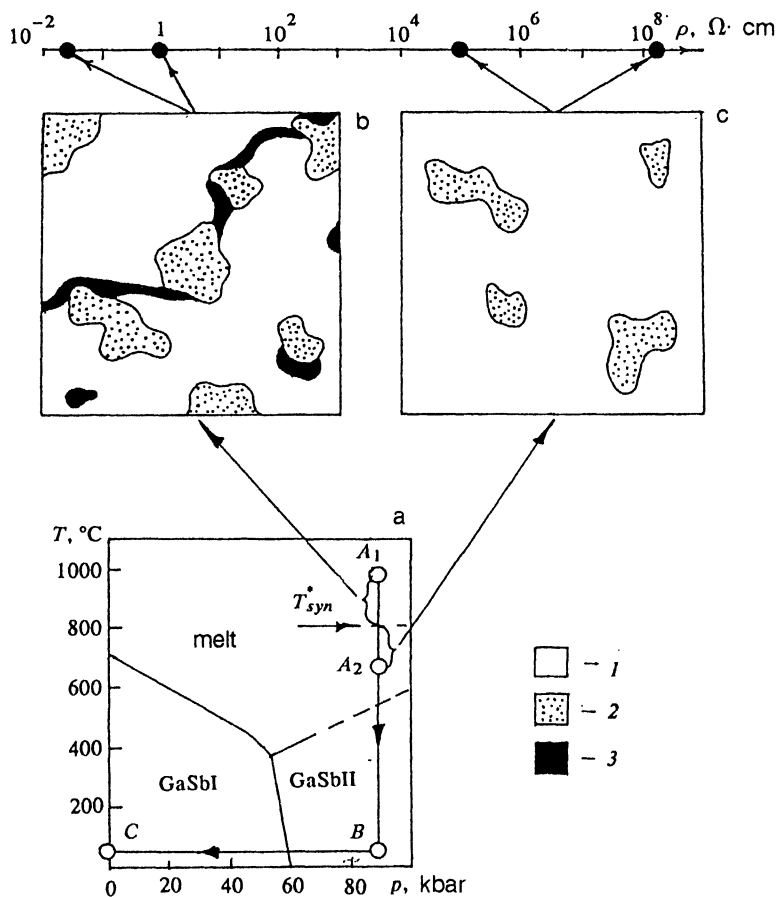
Using the synthesis procedure shown in Fig. 1a, where

FIG. 1. Procedure for synthesizing bulk samples of amorphous gallium antimonide. b, c: Structure of the a-GaSb samples (according to Refs. 7 and 8) produced at various synthesis temperatures. In the synthesis, the original GaSb sample, of stoichiometric composition, was moved across the GaSbI–GaSbII phase-transition line and stopped at p_{syn}. After a hold at T_{syn} (point A), the sample was quenched to room temperature (point B). At this point the pressure was relieved (point C). The process $A_1 \to B \to C$ leads to an amorphous state and a metallic sample; the process $A_2 \to B \to C$ leads to an insulating sample (see the text proper). Frames b and c of this figure correspond to the metallic and insulating samples. Shown for comparison is the electrical-conductivity scale of the insulating and metallic samples at $T = 4.2$ K. The numbers represent inclusions of various phase compositions. 1—The a-GaSb amorphous phase; 2—the c-GaSb crystal; 3—the Ga_xSb_{1-x} phase.

the synthesis temperature T_{syn} was varied at a fixed pressure $P_{syn} = 90$ kbar in order to produce the different a-GaSb samples, we showed in Refs. 5 and 6 that a variation of T_{syn} induces a metal-insulator transition between the two groups of samples. The insulating samples correspond to $T_{syn} < 800°C$, and the metallic ones to $T_{syn} > 800 °C$. The difference in the electrical conductivities of the metallic and insulating samples reaches 10^9 $\Omega \cdot$ cm (Fig. 1).

On the metallic side of the transition (at $T_{syn} \geqslant 800$ °C; Fig. 1b), the resistivity ρ depends only weakly on the temperature. At $T \leqslant 8$ K we see a superconducting transition, in the course of which the resistance decreases smoothly to zero in the interval 1.8 K $\leqslant T \leqslant 8$ K. The absolute value of the resistivity in the normal state is $\rho \sim 0.1–1$ $\Omega \cdot$ cm (Ref. 5, Fig. 1).

According to Refs. 5 and 6, the variation of T_{syn} is accompanied by the following structural changes, which lead to the metal-insulator transition. First, the increase in T_{syn} leads to an increase in the relative content of the tetrahedral crystalline phase GaSb I in the a-GaSb samples, from $\sim 5–10\%$ at $T_{syn} \approx 400$ °C to $\sim 15–17\%$ at $T_{syn} \approx 1100$ °C. Second, at a critical temperature $T^*_{syn} \sim 800$ °C, inclusions of a nonstoichiometric amorphous Ga_xSb_{1-x} phase arise in the interior of the a-GaSb sample. These inclusions have a metallic conductivity, and at $x > 0.5$ they are superconducting. The coexistence of a low-resistivity crystalline GaSb phase and an amorphous, nonstoichiometric Ga_xSb_{1-x} phase in the interior of the

sample leads to the formation of a subnetwork of conducting channels, which shunt the high-resistivity amorphous phase of GaSb and cause a metal-insulator transition. The phase composition of the a-GaSb samples according to the data of Refs. 5 and 6 is shown schematically in Fig. 1, b and c. The typical size of the inclusions can be estimated to be[5] ~ 250 Å.

Since this group of structural disruptions is metastable, it would be natural to expect the presence of the Ga_xSb_{1-x} phase to have a substantial effect on the crystallization of a-GaSb. We need to stress that so far there has been essentially no study of the physical properties of such inclusions. Our purpose in the present study was accordingly to learn about the structural relaxation and crystallization of a-GaSb samples synthesized by quenching under pressure via the procedure shown in Fig. 1a. For this study we selected a-GaSb samples from the metallic side of the metal-insulator transition ($p_{syn} = 90$ kbar, $T_{syn} = 1100$ °C), which exhibit a superconductivity and for which the content of the Ga_xSb_{1-x} phase is maximal (Fig. 1b).

The very possibility of studying an amorphous semiconductor matrix containing metastable submicron-size metallic inclusions is also of interest.

The experimental procedures, including the sample synthesis procedure, are described in detail in Refs. 5 and 6.
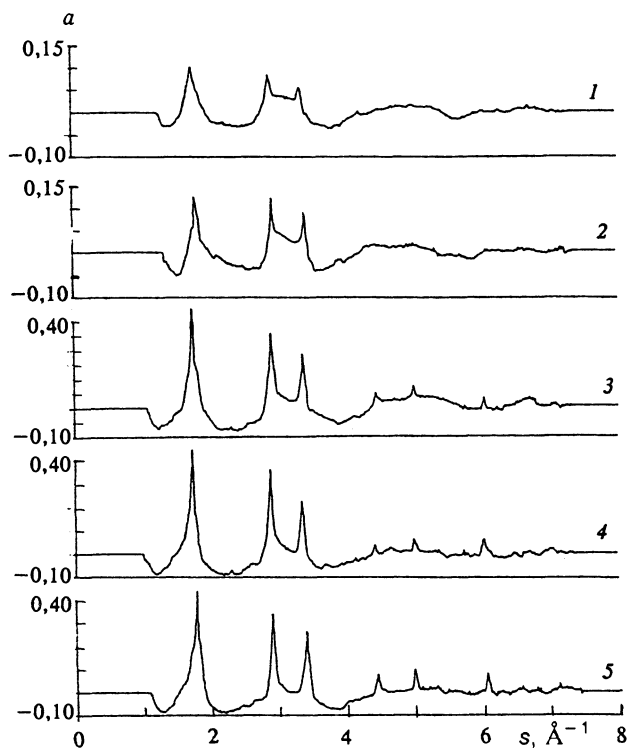
FIG. 2. Change in the structure of metallic a-GaSb samples ($p_{syn}=90$ kbar, $T_{syn}=1100$ °C) in the course of a sequential annealing at various temperatures. *1*—290 K (the original sample); *2*—350; *3*—380; *4*—400; *5*—420 K.

FIG. 3. Structure of the first $a(S)$ peak for a-GaSb. The data shown correspond to the situation after the annealing at 380 K.

2. STRUCTURE OF THE a-GaSb SAMPLES

A computer-controlled microdensitometer of original design was used to analyze the powder diagrams of a-GaSb test samples synthesized by quenching a melt at high pressure ($p_{syn}=90$ kbar, $T_{syn}=1100$ °C) and then subjected to a series of isothermal annealing steps $\sim$50–100 min long in the temperature interval 300–620 K (a "step-by-step crystallization method"). To determine the scattering intensity correctly, we analyzed a plot of the blackening versus the radiation dose. The calibration was tested through independent measurements on certain samples by means of a diffractometer.

Figure 2 shows x-ray scattering structure factors $a(s)$ ($s=4\pi\sin\theta/\lambda$) corresponding to an original a-GaSb sample and to the states reached as the result of each successive isothermal annealing. Values of $a(s)$ were calculated by subtracting the incoherent and instrumental components from the experimental blackening curves of the powder diagrams of the test samples.

We see in Fig. 2 that the spectrum (curve *1* in Fig. 2) corresponding to the original state of the a-GaSb has broad, amorphous peaks. Against the background of these broad peaks are peaks corresponding to crystalline gallium antimonide. The lines of crystalline GaSb, however, are smaller than the amorphous peaks and can be detected reliably in only the first two coordination spheres (curve *1* in Fig. 2). A significant increase in the height of the lines of crystalline GaSb can be seen even in the interval of
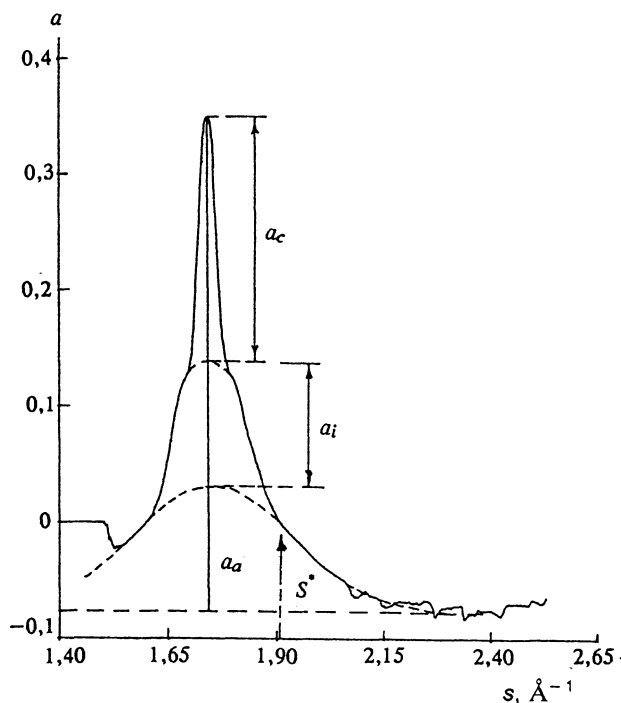
annealing temperatures $T_{ann}\sim$350–380 K (curves *2* and *3* in Fig. 2). A further increase in T_{ann} causes a sharp increase in the height of the lines of crystalline gallium antimonide at $T_{ann}\geqslant$420 K (Fig. 2).

The characteristic temperature $T_{ann}\sim$350–380 K at which the crystalline lines intensify is substantially lower than the crystallization temperature $T_{cr}\sim$420 K found in Ref. 7 by differential thermal analysis of a-GaSb samples produced by quenching under pressure. Approximately the same values of T_{cr} are found for amorphous GaSb films.[8] On the other hand, this feature correlates well with the value of T_{cr} which was revealed for a-GaSb in Ref. 4 by the start of an irreversible decrease in the resistivity ρ of samples in the course of a step-by-step crystallization.

Let us take a closer look at the changes in the structure of the a-GaSb samples during the annealing. As the structure argument s increases, the height of the amorphous peaks decreases significantly (Fig. 2). We thus look at the change in the shape of the first peak in $a(s)$ ($s\sim$1.5–2.2 Å^{-1}), which is a superposition of a crystalline peak and an amorphous one (Fig. 3). Since both the relative heights of these structural particularities and their shapes change with increasing annealing temperature, we adopt the following model for a quantitative description of this process.

It has been shown previously[5] that the shape of a crystalline line can be described well by a Gaussian function $I_c(s)=A_c\cdot\exp(-(s-s_0)^2/\gamma_c^2)$ and that the residual concentration of the crystalline phase in a-GaSb is proportional to $n_c\sim\int I_c(s)ds\sim A_c\gamma_c$.

If we interpret an amorphous peak as a "superbroadened" crystalline line (this is an extremely crude but fre-
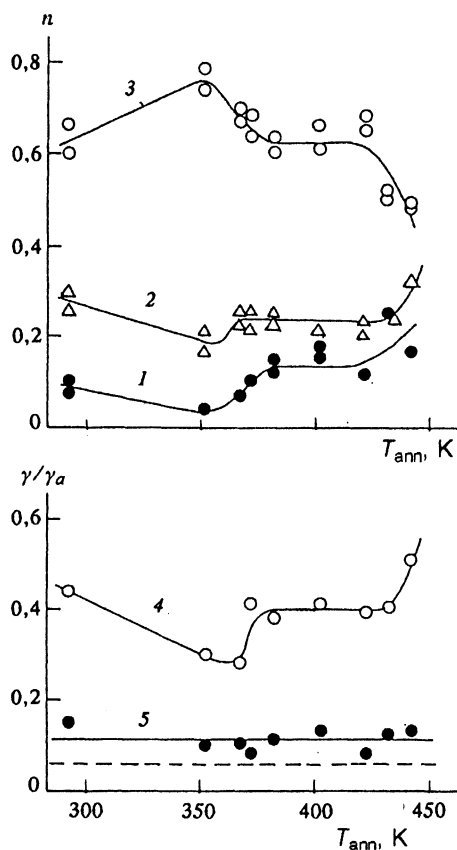
FIG. 4. Behavior of the parameters (*1*) n_c, (*2*) n_a, and (*3*) n_i and the ratios (*4*) γ_i/γ_a and (*5*) γ_c/γ_a. The method for determining the parameters is described in the text proper. The dashed line corresponds to the instrumental limitation on the linewidth.

quently used approximation), we can use the Selyakov formula[9]

$$ L = \frac{0.9\lambda}{\Delta(2\theta)\cos\theta_0} \approx \frac{3.6\pi}{\Delta s} \qquad (1) $$

to estimate the length scale over which the relative order of the amorphous matrix persists. Here λ is the wavelength of the x rays, $\Delta(2\theta)$ and Δs are the half-widths at half-maximum, at θ_0 is the position of the first amorphous peak. It has now been reliably established that formula (1) gives a satisfactory estimate of the length scale of the average order in an amorphous network.[10,11] A calculation from (1) for the case of a-GaSb yields[5] $L \sim 20$ Å.

As expected, however, a Gaussian approximation of the shape of an "amorphous line" turns out to be utterly unsatisfactory. This method is capable of describing only the central region of an amorphous peak. At the edges of the line, at $s \sim s^*$, we find a slope change (Fig. 3), and at $s > s^*$ the decay of the function $a(s)$ steepens substantially. To describe the observed shape of the first peak in $a(s)$ of a-GaSb we accordingly assume that the amorphous part is a superposition of two Gaussian functions, $I_a(s) \sim A_i\exp(-(s-s_i)^2/\gamma_i^2) + A_a\exp(-(s-s_a)^2/\gamma_a^2)$,

with $\gamma_i < \gamma_a$, that the first term describes the region of the amorphous peak, and that the second term describes the edge of the line.

In this model, $a(s)$ near $s \sim 1.5$–2.2 Å^{-1} is thus given by

$$ a(s) = A_c\exp\left(-\frac{(s-s_c)^2}{\gamma_c^2}\right) + A_i\exp\left(-\frac{(s-s_i)^2}{\gamma_i^2}\right) $$
$$ + A_c\exp\left(-\frac{(s-s_a)^2}{\gamma_a^2}\right). \qquad (2) $$

At first glance it would appear that Eq. (2) has too many adjustable parameters. In the case of a-GaSb, however, the analysis of the experimental $a(s)$ curve simplifies substantially. In the first place, at annealing temperatures $T_{ann} \leqslant 450$ K the parameters s_c, s_i, and s_a, which specify the positions of the lines and the widths γ_c and γ_a are constant. By virtue of the relation $|s_c - s_i|$, $|s_c - s_a| \leqslant s_c$, the experimental amplitude of the change in the structure factor, Δa_{max}, gives us an additional relationship $\Delta a_{max} = A_c + A_i + A_a$. In addition, treating this model as a simplified version of correlation analysis for determining the concentrations of components in a limited interval of the structural argument, $s < 2.5$ Å^{-1} (Ref. 5), we introduce the parameters n_a, n_i, and n_c, which are relative concentrations:

$$ n_{a,i,c} = \frac{A_{a,i,c}\gamma_{a,i,c}}{A_a\gamma_a + A_i\gamma_i + A_c\gamma_c}. \qquad (3) $$

Here $n_a + n_i + n_c = 1$. Taking this relation into account, we easily see that when using Eq. (2) two adjustable parameters are sufficient to approximate the experimental data, and the corresponding mathematical procedure turns out to be comparatively straightforward. It can be seen from Fig. 3 that the method used here leads to a good description of the shape of the first $a(s)$ peak.

Figure 4 shows the changes in the parameters n_a, n_i, n_c, γ_i, and γ_c during the annealing process. The annealing at $T_{ann} \sim 350$ K raises n_a, while it reduces n_c, n_i and γ_i. With further annealing in the temperature interval 350 K $\leqslant T_{ann} \leqslant 380$ K, there is some decrease in n_a, while there are increases in n_i and n_c. At the same time, at $T_{ann} \sim 370$ K the parameter γ_i increases sharply. In the region $380 \leqslant T_{ann} \leqslant 430$ K there is a slight increase in the concentration n_c of the crystalline phase, while at $T_{ann} > 430$ K a crystallization growth of n_c begins. This growth is accompanied by an increase in n_i and a decrease in n_a. Within the experimental errors, the parameter γ_c remains essentially constant.

Let us examine a possible physical interpretation of the various contributions to Eq. (2). We first note that the behavior of n_i during the annealing is qualitatively the same as that of n_c (Fig. 4). This agreement suggests that the contribution with the subscript i is related to the crystalline phase. Furthermore, in the initial stage of the annealing ($T_{ann} < 350$ K) the crystal density decreases, and n_a increases. If we identify this process as the structural relaxation characteristic of most amorphous materials,

including[4] a-GaSb, then it is natural to link the decrease in n_c with an additional disordering of the system as a result of a stress relaxation at the interfaces between the amorphous and crystalline phases. Consequently, the value of n_a and the corresponding contribution to Eq. (2) reflect the presence of specifically the a-GaSb amorphous phase. This suggestion is in agreement with the decrease in n_a with the onset of intense crystallization ($T_{\text{ann}} > 430$ K).

This analysis suggests that the contribution with subscript i reflects the existence of a transitional region between the crystalline inclusions and the amorphous matrix, and that n_i corresponds to the volume fraction of this boundary region. This assumption leads to natural explanation of the complex changes in $n_c(T_{\text{ann}})$ and $n_i(T_{\text{ann}})$ (Fig. 4).

In this model, the parameter γ_a is determined by the correlation length L_a of the disordered amorphous network of a-GaSb, γ_c is determined by the crystallite size L_c, and γ_i is determined by the size (L_i) of the transition region from the ordered arrangement of atoms in a crystallite to the disordered arrangement in the amorphous network. Using Eq. (1) and the data on $a(s)$ (Fig. 2), we find the estimates $L_a \approx 20$ Å $=$ const, $L_c \sim 200$ Å, and $L_i \sim 50$ Å.

Interestingly, the value of γ_c and thus that of L_c remain essentially constant during the annealing process (Fig. 4). At $T \leqslant 450$ K, the formation of c-GaSb nanocrystals thus dominates the crystallization of a-GaSb. With a further increase in annealing temperature, $T_{\text{ann}} > 450$ K, the typical size of the c-GaSb crystallites begins to increase, while the parameter γ_c decreases. Unfortunately, we were able to follow the growth process only to $L_c \sim 400$ Å because of limitations imposed by the apparatus (Fig. 4).

Further evidence in favor of this proposed interpretation of the structural data on a-GaSb comes from the relations among the contributions to $a(s)$ characterized by the parameters s_c, s_i, and s_a. For all annealing temperatures, the inequality $s_c > s_i \approx s_a$ holds for a-GaSb, and the corresponding difference is $s_c - s_a \sim 0.025$ Å^{-1}. This relation probably stems from an effective increase in the interatomic distances from that of the crystal, due to the scatter in the bond lengths and angles in the a-GaSb amorphous phase.

It follows from the data in Fig. 4 that the crystallization of a-GaSb occurs in two steps. The first region, with an increase in n_c and n_i, is observed in the range 350 K $\leqslant T \leqslant 380$ K, while the second is observed at $T_{\text{ann}} > 430$ K. Interestingly, in both temperature ranges there is a sharp decrease in the size of the boundary region (the parameter γ_i increases). This behavior indicates that processes at the boundaries of inclusions play a dominant role in the crystallization of the metastable phases of a-GaSb. According to Refs. 7 and 8, a nonstoichiometric amorphous Ga_xSb_{1-x} phase exists at the interface between the amorphous and crystalline phases (Fig. 1). One might suggest that the changes in the boundary region (Fig. 4) and the associated changes in the phase composition of the sample (Fig. 4) can be attributed at least in part to the Ga_xSb_{1-x} phase.
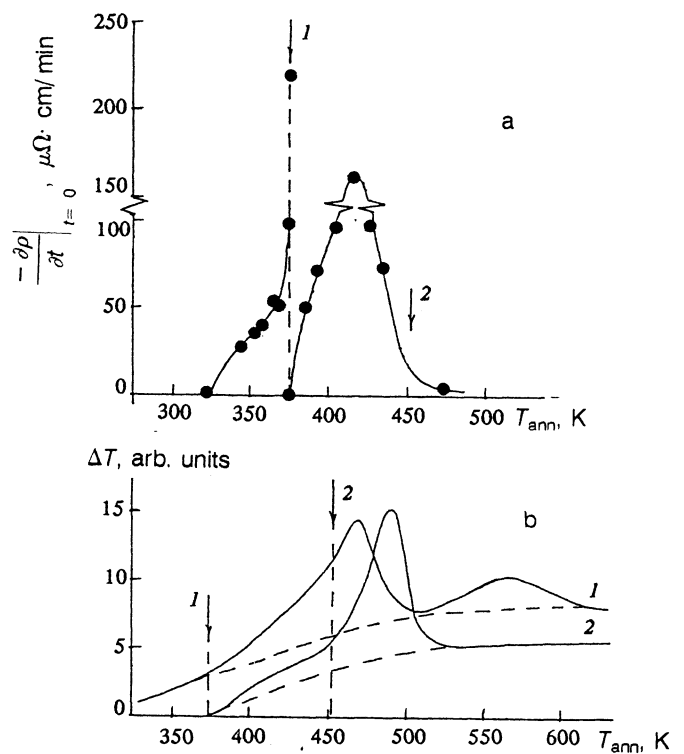

FIG. 5. a: Change in the rate of the resistance relaxation for various annealing temperatures. b: Heat-release curves for (1) a metallic GaSb sample and (2) an insulating sample. The dashed lines are the baselines in the DTA method. The arrows show characteristic temperatures: 1—A structural anomaly (370 K); 2—the end of the pronounced changes in resistance (450 K).

3. STABILITY REGION AND KINETICS OF PHASE TRANSITIONS OF THE METASTABLE PHASES IN a-GaSb

The structural-analysis procedure used in the preceding section of this paper is most effective in that region of annealing temperatures in which the amplitudes A_i, A_a, and A_c are of the same order of magnitude. Since there is a transition at $T_{\text{ann}} \geqslant 450$ K from $A_c \sim A_i$, A_a to $A_c \gg A_i$, A_a, it is not possible to carry out a reliable analysis of the changes in the phase composition of the samples, including the evolution of the boundary region. We accordingly studied the crystallization and relaxation of a-GaSb by other methods: by differential thermal analysis (DTA) $\rho(T,t)$ and by measuring the temperature and time dependences of the electrical conductivity of the samples.

In the resistance measurements, the kinetics of the phase transitions was studied on the basis of $\rho/\rho_0 = f(t)$ relaxation curves [$\rho_0 = \rho(t=0)$] recorded in a series of isothermal annealing steps in the temperature interval 300–600 K. In addition, we measured the temperature dependence of the resistivity in the interval from $T = 1.8$ K to $T = T_{\text{ann}}$ before each successive annealing at a fixed temperature T_{ann} higher than that of the preceding annealing. We also recorded the field dependence of the magnetoresistance $\rho(H,T)$. Galvanomagnetic characteristics of a-GaSb samples recorded in these experiments will be discussed in the following section of this paper.

If we treat ρ as a function of the concentration of the metastable phase (V), i.e., $\rho = f(V)$, then in the initial stage of the annealing, in which the changes in V are not very large $[V_0 - V(t) \ll V_0, \ V_0 = V(t=0)]$, we can write

$$\frac{\partial \rho}{\partial t} \approx \frac{\partial f}{\partial V}\bigg|_{V=V_0} \frac{\partial V}{\partial t}. \tag{4}$$

In the Avrami–Kolmogorov approximation[12] we have

$$V = V_0 \exp\left(-\left(\frac{t}{\tau}\right)^n\right), \tag{5}$$

and

$$\frac{\partial \rho}{\partial t} \cong -n \frac{\partial f}{\partial V}\bigg|_{V=V_0} \frac{t^{n-1}}{\tau^n} V. \tag{6}$$

It follows from (6) that we can estimate the Avrami exponent n by analyzing the behavior of $\partial \rho / \partial t$ in the limit $t \to 0$.

We find $0 < \partial \rho / \partial t|_{t=0} < \infty$ over the entire range of annealing temperatures studied in the limit $t \to 0$. This result corresponds to the case $n \approx 1$.

Figure 5a shows the experimental $\partial \rho / \partial t|_{t=0}$ dependence. It was found that holds the entire range of annealing temperatures studied the relation $\partial \rho / \partial t < 0$. Two regions of the variation of $\partial \rho / \partial t$ can be distinguished. First (at $T_{ann} < 370$ K), the absolute value of the rate of change of the resistivity increases with the temperature. It reaches a maximum at $T_{ann} \approx 370$ K. Repeated isothermal annealings at this temperature initially lead to a pronounced increase (by a factor of more than 2) in $|\partial \rho / \partial t|$; then, after a long hold at $T_{ann} \approx 370$ K, $\rho(T_{ann}, t)$ reaches a steady-state value, and we have $\partial \rho / \partial t \approx 0$. As the annealing temperature is raised further, the derivative $|\partial \rho / \partial t|$ initially increases, goes through a maximum at $T_{ann} \sim 410$ K, and then decreases.

The function $f(V)$ is not known accurately for a complex multicomponent system. It is thus difficult to carry out a quantitative analysis of the experimental data on $\rho(t)$ on the basis of Eqs. (4)–(6). Qualitatively, however, the existence of two temperature ranges in which $\partial \rho / \partial t$ changes sharply is correlated with data from the x-ray diffraction analysis (Fig. 4), where we again see two regions of an increase in $n_c(T_{ann})$, at $T_{ann} \sim 370$ K and $T_{ann} \sim 430$ K.

We turn now to the results found by differential thermal analysis.

Figure 5b shows typical curves of the heat evolution for metallic a-GaSb samples (samples containing inclusions of the nonstoichiometric amorphous Ga_xSb_{1-x} phase) and for insulating samples, in which there are essentially no nonstoichiometric inclusions (curves 1 and 2, respectively). For the sample on the metallic side of the metal-insulator transition, the main heat release-peak is substantially broadened, and it lies about 30 K below the heat release-peak for the insulating sample. Another distinctive feature of the DTA curves for the metallic a-GaSb samples is the presence of an additional broad peak at $T_{ann} \sim 550$–600 K.

Working from data on the structure of the a-GaSb samples found in previous studies[5,6] (see also Fig. 1), and comparing curves 1 and 2 in Fig. 6b, we might suggest that the presence of the nonstoichiometric amorphous Ga_xSb_{1-x} phase leads to structural features on the DTA curves in two distinct temperature intervals: $T_{ann} \sim 370$–430 K (there is a broadening of the DTA peak as a result) and $T_{ann} \sim 500$–620 K (this is the additional heat-release peak). The main heat-release peak in Fig. 5b is evidently due to a crystallization of the amorphous phase proper of a a-GaSb.

Working from the area under the heat-release peaks on the DTA curves, we estimated the heat of crystallization Q. For the main peak, Q turns out to be 12–16 kJ/mole, while for the additional peak in the case of the metal sample it is 7 ± 2 kJ/mole. For the case of the main peak, we used a method involving scanning at different rates[13] to find the activation energy for crystallization and the Avrami exponent. For the metal samples we found $E_a \approx 1.2 \pm 0.2$ eV, and for the insulating samples $E_a \approx 1.4 \pm 0.2$ eV. In both cases the Avrami exponent was $n \approx 1 \pm 0.1$. The value found for E_a agrees with data found in Ref. 4.

According to the present understanding,[12] a value $n \approx 1$ reflects a lowered dimensionality of the growth and corresponds to either a quasi-$1D$ growth of crystallites or a diffusion-controlled growth at grain boundaries. In the case of a-GaSb, the latter possibility looks more likely, since the crystallization process is accompanied by a restructuring of the boundary region according to the structural data (Fig. 4).

We can use these results to analyze the possible nature of the two crystallization processes in a-GaSb, at $T_{ann} \sim 370$ and > 430 K. Comparing the characteristic temperature $T_{ann} \sim 370$ K (the structural anomaly; the sharp peak in $-\partial \rho / \partial t$) and $T_{ann} \sim 450$ K (the end of the relaxation of the electrical conductivity; $\partial \rho / \partial t = 0$) with the DTA curve for the metallic sample, we find that a significant heat release begins after the first crystallization process has been completed. We also find that the crystallization of a-GaSb continues after the value $\partial \rho / \partial t = 0$ is reached.

At $T_{ann} > 430$ K, the crystallization of the tetragonal amorphous phase proper of a-GaSb is evidently predominant. The termination of the changes in the resistance can easily be explained on the basis that a threshold n_c^* for percolation through the low-resistivity crystalline phase has been reached. It follows from the data in Fig. 4 that at $T_{ann} > 370$ K the system is near the percolation threshold for $3D$ case: $n_c \sim n_c^* = 0.15$–0.17.

No significant heat evolution is observed for the first crystallization region ($T_{ann} \sim 370$ K; Fig. 5). This result indicates that a low volume fraction of the metastable phase crystallizes in this temperature interval. The changes in the conductivity in this region, on the other hand, are fairly large.

This behavior can apparently be explained by assuming that the first crystallization process results from crystallization of the nonstoichiometric amorphous Ga_xSb_{1-x} phase. The slight heat release would then be due to the low
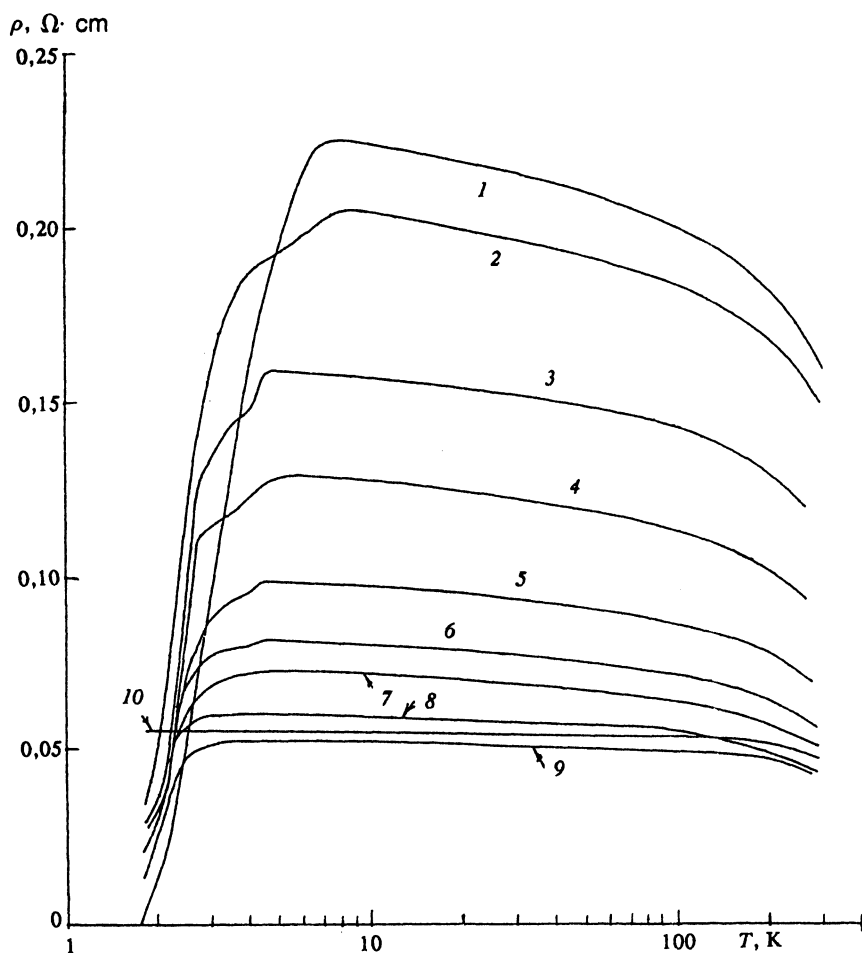
FIG. 6. Change in the superconducting transition of a-GaSb in the course of sequential isothermal annealing steps at various temperatures. 1—290 K (original sample); 2—360; 3—370; 4—400; 5—420; 6—440; 7—450; 8—470; 9—520; 10—570 K.

concentration of regions with deviations from stoichiometry (according to Refs. 5 and 14, the volume fraction of the superconducting Ga_xSb_{1-x} inclusions is no greater than 3–5%), and the significant changes in ρ would be due to changes in the subnetwork of conducting channels (Fig. 1) which shunt the electrical conductivity of the metallic samples.

Comparison of the DTA data with the x-ray diffraction data shows that the interval of annealing temperatures 380–430 K, in which the structural changes are small, is anomalous. Specifically, in the region with n_c, n_i, $n_a \approx$ const (Fig. 4) there is a substantial heat release (Fig. 5b): No less than 23% of the area under the DTA curve, which is proportional to the latent heat of phase transition, corresponds to this temperature interval. The nature of this anomaly will be discussed below.

4. SUPERCONDUCTIVITY OF METASTABLE PHASES IN AMORPHOUS GALLIUM ANTIMONIDE

Since superconductivity arises in amorphous gallium antimonide because of the presence of the Ga_xSb_{1-x} phase with $x > 0.5$ (Refs. 5 and 6), a study of the evolution of the superconducting properties of a-GaSb makes it possible to test and refine the results found in the preceding sections of this paper.

Figure 7 shows the changes in the resistance characteristics of the superconducting transition of a-GaSb in the

course of the annealing process. The width of the superconducting transition in the original sample (curve 1) is significantly greater than the widths which are customarily observed: The resistivity decreases smoothly to zero in the interval $1.8 < T < 8$ K. The reason for this behavior is a scatter in the composition of the nonstoichiometric inclusions and a resultant scatter in transition temperature T_c (Ref. 15). As a result, a superconductivity of the inclusions with the highest transition temperature arises at $T_c = T_m \sim 8$ K. As the temperature is lowered, the resistance of the inclusions for which the condition $T_c > T$ holds vanishes; at $T = T_p$ an infinite cluster forms from the superconducting inclusions, and a state of the sample with $\rho = 0$ is established. The percolation nature of the superconducting transition was analyzed in detail in Refs. 5 and 14.

As the annealing temperature is raised, the absolute value of the resistivity $\rho(T > T_m)$ decreases, and the superconducting structural features simultaneously shift down the temperature scale (Fig. 6). A state with $\rho = 0$ is not reached after the annealing at $T_{ann} \sim 330$–340 K; the resistivity remains nonzero over the entire studied temperature range $T \geqslant 1.8$ K.

It is clear from the data on the resistance of the sample as a function of the annealing temperature (Fig. 7a) that the metastable superconductivity of the Ga_xSb_{1-x} inclusions is annealed out in two steps. First, at an annealing

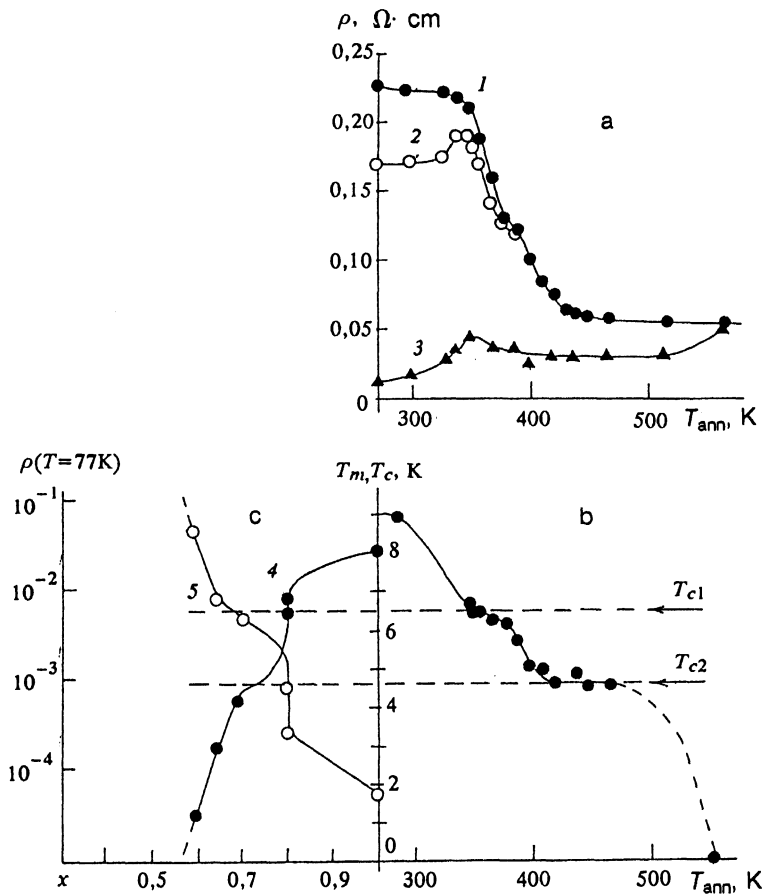FIG. 7. a: The electrical conductivity of a-GaSb samples as a function of the annealing temperature. 1—The measurements of ρ were carried out after an annealing step at 10 K; 2—4.2; 3—2 K. b: Evolution of the characteristic transition temperature of the inclusions during the annealing. c: Changes in the transition temperature (4) and the resistivity at $T=77$ K (5) as the composition of the Ga_xSb_{1-x} inclusions is varied. The experimental data on $T_c(x)$ and $\rho(x)$ were taken from Ref. 15.

temperature $T_{ann} \sim 370$ K, the superconductivity of the inclusions for which the transition temperature satisfies 4 K$\leqslant T_c \leqslant 10$ K is suppressed. In the interval of annealing temperatures $T_{ann} > 370$ K, the curves of $\rho(T=10$ K$)$ and $\rho(T=4.2$ K$)$ (1 and 2 in Fig. 7a) essentially coincide. The superconductivity of the inclusions with $T_c < 4$ K persists over the interval of annealing temperatures $370 < T_{ann} \leqslant 560$ K. A complete suppression of the superconducting particularities is reached after an annealing at $T_{ann} > 560$ K (compare curves 3 and 1 in Fig. 7a). A complete annealing of the metastable superconductivity of a-GaSb thus occurs after the tetrahedral amorphous phase of gallium antimonide has crystallized completely (Fig. 5).

It follows from Fig. 6 that the evolution of the superconducting properties can conveniently be characterized by the value of T_m, which corresponds to the highest superconducting transition temperature of the inclusions for the given state of the sample, reached in the sequence of isothermal annealing steps.

It can be seen from Fig. 7b that in the annealing-temperature interval $290 \leqslant T_{ann} \leqslant 350$ K the value of T_m decreases from $T_m \sim 9$ K to $T_m = T_{c1} \approx 6.5$ K. An increase in the annealing temperature in the interval 350–380 K does not change the value of $T_m = T_{c1}$. With a further increase in the annealing temperature, at $380 \leqslant T \leqslant 430$ K, the transition temperature T_m decreases to $T_m = T_{c2} \approx 4.5$ K. In the interval $430 < T_{ann} < 500$ K, T_m then remains

essentially constant at $T_m = T_{c2}$. Superconductivity is completely suppressed at $T_{ann} > 500$ K (Fig. 7b).

Working from results of the present study (Fig. 7b) and from data in the literature on the behavior of the superconducting properties of the Ga_xSb_{1-x} phase,[15] we can reconstruct the concentration dependence of the transition temperature and that of the electrical conductivity of the inclusions, $T_c(x)$ and $\rho(x)$. We can also determine the typical values of x corresponding to the two components of the nonstoichiometric amorphous phase, which differ in physical properties (Fig. 7c). It follows from the data on $T_c(x)$ that at $T \leqslant 350$ K the superconductivity of inclusions with $x > 0.8$ vanishes. These inclusions contain the maximum amount of gallium in the Ga_xSb_{1-x} phase, and they have the highest transition temperature. The stablest inclusions are those with $x \approx 0.8$–0.7, with a maximum transition temperature $T_c \sim 4$ K. The superconductivity of inclusions of this type can be suppressed by annealing at $T_{ann} \sim 570$ K (Fig. 5b).

We suggest that the values of T_c in the interval $T_{c2} \leqslant T_c \leqslant T_{c1}$ correspond to a transition region near $x \sim 0.8$ and that the range of concentrations over which inclusions with these characteristics exist is fairly narrow. As a result, the transition temperatures for the first component of the Ga_xSb_{1-x} phase $(x > 0.8)$ are in the interval $6.5 \leqslant T_c \leqslant 8$ K, while those for the second component $(x \leqslant 0.8)$ have an upper limit $T_c \sim 4.5$ K. The physical reason for this $T_c(x)$
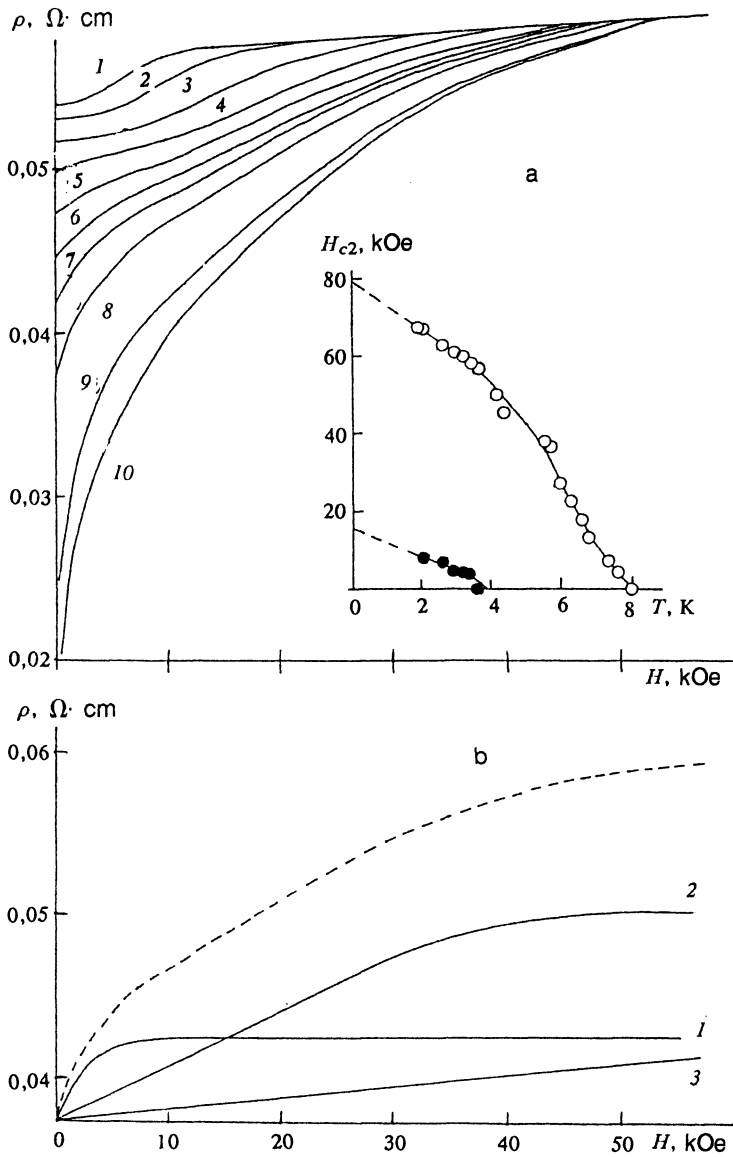
FIG. 8. a: Field dependence of the resistivity, $\rho(H)$, for the original, unannealed, metallic a-GaSb sample at various temperatures. 1—6.6 K; 2—6.3; 3—5.5; 4—4.1; 5—3.5; 6—3.2; 7—2.9; 8—2.6; 9—2.1; 10—1.9 K. The inset shows the temperature dependence of the critical field H_{c2} for inclusions with $x > 0.8$ (open circles) and $x < 0.8$ (filled circles). b: Field dependence of the magnetoresistance for $T = 2.6$ K.

behavior may be a change in the short-range order of the Ga_xSb_{1-x} phase. Near $x \sim 1$ in Ga_xSb_{1-x}, the structure of amorphous gallium should be predominant, while at $x \sim 0.5$ the distinct tetrahedral structure of GaSb should be predominant. There must accordingly be a critical concentration which corresponds to a transition from one of these types of short-range order to another, at which the physical characteristics of this system may have a structural feature, e.g., jumps in the values of T_c and ρ (Fig. 7c). Looking at Fig. 7, we might suggest that this structural transition for Ga_xSb_{1-x} occurs at $x \approx 0.8$.

Further information on the nature of the superconductivity of a-GaSb was found through an analysis of the field and temperature dependence of the magnetoresistance, $\Delta\rho/\rho = f(H,T)$, and the evolution of this behavior in the course of the annealing process. It has been shown previously[5] that the positive magnetoresistance of a-GaSb at $T < T_m$ stems primarily from a disruption of the superconductivity of the inclusions, while the contribution of the standard kinetic mechanisms is small because of the low

mobility μ. The condition $\mu H \ll 1$ holds in the magnetic field interval $H < 150$ kOe (Ref. 5).

Figure 8a shows the variation of the field dependence of the resistivity $\rho(H)$ with the temperature for the original (unannealed) sample. At $T \leqslant 4$ K the $\rho(H)$ curve acquires a more complex shape. The experimental curve has two regions which correspond to the disruption of two distinct superconducting phases, with different critical fields H_{c2}. After the disruption of the superconductivity by the magnetic field has come to a halt, there is a slight linear increase in the resistivity of the sample with the magnetic field (Fig. 8a).

In general, the data on $\rho(H)$ can thus be described by a superposition of several contributions (Fig. 8b, curves 1–3). For $T \leqslant 4$ K, there is a first a disruption of the inclusions with the lowest critical properties, and the corresponding component of the $\rho(H)$ curve reaches saturation (curve 1). The component corresponding to the other superconducting phase, with higher critical properties (curve 2), behaves in a similar way. The third component of the

$\rho(H)$ curve corresponds to a linear asymptotic behavior which is observed in strong magnetic fields. This component is apparently due to a magnetoresistance of the non-superconducting a-GaSb matrix. At $T > 4.2$ K, two components are evidently sufficient to describe the $\rho(H)$ curve (these components are the analogs of curves 1 and 3 in Fig. 8b).

Following Ref. 5, we define the field H_{c2} for the first superconducting phase as the field at which $\rho(H)$ starts its linear asymptotic behavior, while we define H_{c2} for the second superconducting phase as the field at which the initial region of rapid variation of the $\rho(H)$ curve comes to a halt (Fig. 8). We can then separate the components of the $\rho(H)$ curve and reconstruct curves of the critical fields $H_{c2}(T)$ for the two superconducting phases (see the inset in Fig. 8a).

Extrapolating $H_{c2}(T)$ to the H and T axes, we find the characteristic values $H_{c2}(T)$ and $T_c(H=0)$ for the first superconducting phase: $T_c \approx 8$ K and $H_{c2}(0) \approx 80$ kOe. The corresponding properties for the second phase are $T_c \approx 4$ K and $H_{c2}(0) \approx 14$ kOe.

The values found for T_c in this manner are close to those found from the change in T_m in the course of the annealing (Fig. 7). It is natural to link the small differences with the uncertainty in the determination of T_c for a complex disperse system by the different methods.

The value $H_{c2}(0) \approx 80$ kOe for the first phase agrees with the value of $H_{c2}(0)$ for amorphous gallium, which is[16] ~ 100 kOe. The high values of $H_{c2}(0)$ for the second phase seem to rule out the possibility of interpreting this structural peculiarity of the positive magnetoresistance of a-GaSb on the basis that there are inclusions of a high-pressure ordered metallic phase of GaSb or of metastable superconducting phases of antimony in the interior of the sample (the losses of the components during the synthesis of the a-GaSb can be ignored,[5] since regions with excess gallium would imply the presence of inclusions with a local excess of antimony). It can be seen in the literature[17,18] that these phases have transition temperatures close to those observed for a-GaSb, but their critical fields H_{c2} are much lower, no greater than ~ 5 kOe.

The parameter T_m and the corresponding quantity H_{c2} which were introduced above are characteristics of a superconducting inclusion with the maximum transition temperature and maximum critical field. If there is a scatter in the superconducting properties, the specification of T_m is not sufficient to completely describe the system of superconducting inclusions. If we introduce a distribution function of the volume of inclusions with respect to transition temperature, $\varphi(T_c)$, then the volume of the sample occupied by a superconducting phase at the given temperature is given by

$$V_s(T) = \int_T^\infty \varphi(T_c)dT_c, \qquad (7)$$

where $\varphi(T_c \geqslant T_m) \equiv 0$. It can be shown[19] that for a-GaSb the magnetoresistance is described by $\Delta\rho/\rho \sim V_s(T)$ in a first approximation (this condition holds except in a small neighborhood of the temperature T_p, at which an infinite
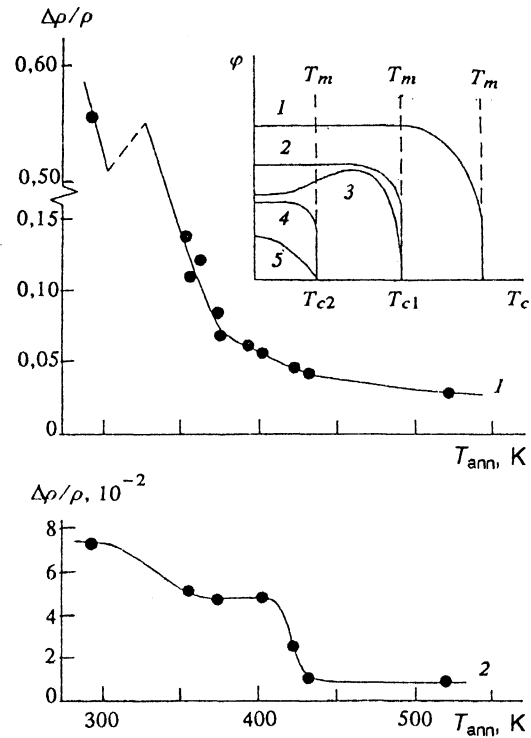

FIG. 9. Change in the magnetoresistance in a field $H=45$ kOe in the course of the annealing process. 1—Measurements at $T=2$ K; 2—4.2 K.

cluster is formed from the superconducting inclusions). By analyzing the behavior of $\Delta\rho/\rho$ in a fixed magnetic field, one can thus determine the behavior of V_s and $\varphi(T_c)$ in the course of the annealing process (Fig. 9).

We first note that the curve of $\Delta\rho/\rho = f(T_{ann})$ measured at the lowest temperature, $T \sim 2$ K (curve 1 in Fig. 9), reflects a complete change in the volume of the sample which is occupied by superconducting phases of a-GaSb. We see that in the course of the annealing the value of $\Delta\rho/\rho$ and thus that of V_s fall off monotonically.

The data found on $\Delta\rho/\rho = f(T_{ann})$ at $T \sim T_{c1} \sim 4$ K evidently tell us the changes in the volume V_s caused by the annealing of predominantly the first superconducting phase of Ga_xSb_{1-x}, with $x > 0.8$ ($T_c \geqslant 6.5$ K). It follows from Fig. 9 (curve 2) that annealing at $T_{ann} \sim 350$ K leads to a change in the volume of the inclusions with $x > 0.8$. Later on, at $T_{ann} \sim 370$ K, the rate of crystallization of this nonstoichiometric amorphous phase decreases. As the annealing temperature is raised to $T_{ann} \sim 400$–430 K, the superconducting inclusions with $x > 0.8$ disappear, and the superconductivity of a-GaSb is thereafter due primarily to Ga_xSb_{1-x} inclusions with $x < 0.8$.

Using the data found here (Figs. 7 and 9), we can qualitatively determine the evolution of the function $\varphi(T_c)$ in the course of the annealing (see the inset in Fig. 9). In the original state (curve 1), the distribution of inclusions with respect to transition temperature has a limit $T_m \sim 9$ K. Annealing at $T_{ann} \sim 350$ K reduces T_m to $T_m = T_{c1} \approx 6.5$ K and may also reduce the amplitude of φ,
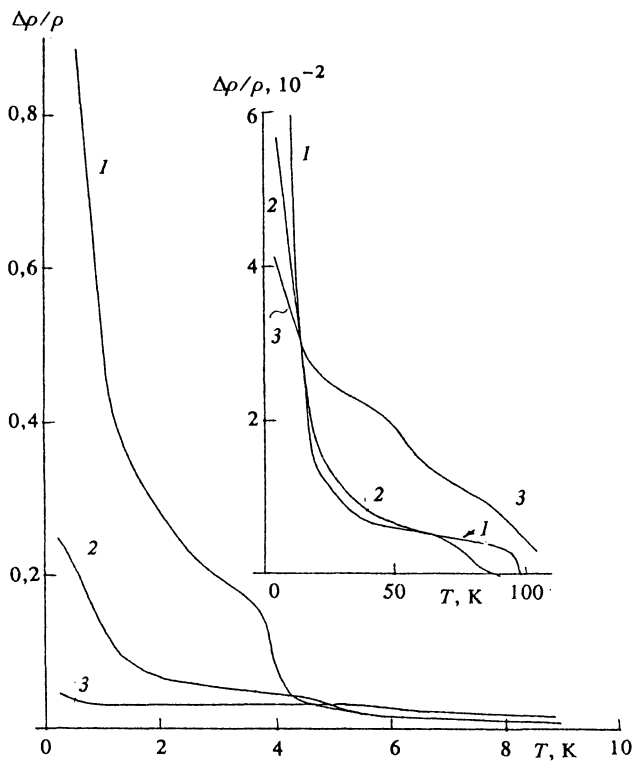
FIG. 10. Temperature dependence of the magnetoresistance of a-GaSb in a field $H=133$ kOe at various stages in the annealing process. 1—Original sample; 2—annealing at $T=420$ K (the phase with $x>0.8$ has crystallized completely); 3—620 K (the metastable phases of a-GaSb have crystallized completely).

since the volume of superconducting phase in the sample decreases (curve 2).

Annealing in the interval $350 \leqslant T_{ann} \leqslant 380$ K does not alter T_m, while it causes a small change in the volume of inclusions with $x>0.8$. The total volume of superconducting phase, on the other hand, continues to decrease. As a result, the value of φ decreases in this interval of annealing temperatures, primarily in the interval $T_c < T_{c2}$ (curve 3).

An increase in the annealing temperature to $T_{ann} \sim 380$–430 K leads to a sharp decrease in T_m, to $T_m = T_{c2} \approx 4.5$ K, and to a decrease in the amplitude of φ (curve 4). A further annealing, up to $T_{ann} \sim 500$ K, occurs at $T_m =$ const, with a decrease in φ. The volume of the inclusions with $x<0.8$ also decreases (curve 5). At $T_{ann} > 500$ K, we observe a complete suppression of the superconducting properties of a-GaSb.

In the schematic description of the distribution function $\varphi(T_c)$, we assumed that $\varphi(T_c)$ depends weakly on the temperature at $T < T_m$ (Ref. 14).

We conclude this section of the paper with a look at how the annealing affects the high-temperature structural particularity of the magnetoresistance of a-GaSb (Refs. 5 and 19), which is manifested in a long region of a decrease in $\Delta\rho/\rho$ with the temperature at $T > T_m$ (Fig. 10). An important point is that near $T \sim 100$ K the magnetoresistance decreases sharply to $\Delta\rho/\rho \approx 0$ or even changes sign.[5,19] Working from this behavior of the $\Delta\rho/\rho(T)$

curve, and also taking account of the condition $\mu H \ll 1$, under which we can ignore the Lorentzian contribution to the positive magnetoresistance over the entire temperature range studied, we asserted in Ref. 19 that this structural particularity of $\Delta\rho/\rho$ was due to a high T_c superconductivity of a-GaSb with $T_c \sim 100$ K.

However, the data in Fig. 10 contradict this explanation of the high-temperature anomaly. In the region $T < T_m$, a sequential annealing suppresses the positive contribution to the magnetoresistance, as would be expected on the basis of a model which links the superconductivity of a-GaSb with inclusions of an amorphous Ga_xSb_{1-x} phase. On the other hand, at $T > T_m$, an annealing at $T \sim 420$ K, which leads to the crystallization of inclusions with $x>0.8$, spreads out the structural feature at $T \sim 100$ K and increases the value of $\Delta\rho/\rho$ at $T \sim 70$ K (curve 2 in Fig. 10). A complete crystallization of the metastable phases of a-GaSb causes a further increase in $\Delta\rho/\rho$ at $T > T_m$ (curve 3 in Fig. 10).

Consequently, the change caused in $\Delta\rho/\rho$ at $T > T_m$ by the annealing rules out an explanation of the structural feature in the magnetic resistance at $T \sim 100$ K on the basis of a high T_c superconductivity. On the other hand, the suppression of the feature at $T \sim 100$ K during annealing indicates that this anomaly is related to the presence of the Ga_xSb_{1-x} phase and/or a change in the structure of the boundary between the amorphous and crystalline phases. The specific mechanism responsible for the appearance of the structural particularity of $\Delta\rho/\rho$ at $T \sim 100$ K remain unresolved.

5. DISCUSSION OF RESULTS

The experimental data found in the present study establish the sequence of phase transitions and the resultant changes in the structure and composition of metallic samples of amorphous gallium antimonide in the course of the crystallization ($T_{syn} = 1100$ °C, $p_{syn} = 90$ kbar).

In the initial stage of the annealing, at $T_{ann} \leqslant 350$ K, a precrystallization process takes place. It involves a decrease in the relative size of the crystalline regions, n_c, and a blurring of the boundary region between the amorphous and crystalline phases. The characteristics of the least stable inclusions, of the Ga_xSb_{1-x} phase with $x \sim 1$ change simultaneously, and the maximum value of x decreases to $x \sim 0.8$. This process could apparently be caused by a relaxation of residual stress in the a-GaSb sample, since we would expect the greatest stress in the amorphous GaSb network to occur at the boundaries of regions with a maximum deviation from stoichiometry, where the short-range order changes most sharply.

In the interval 350 K $\leqslant T_{ann} \leqslant 380$ K the metastable phases of a-GaSb begin to crystallize. This crystallization can be linked with a crystallization of the Ga_xSb_{1-x} phase with $x<0.8$. The maximum superconducting transition temperature, which limits the distribution function $\varphi(T_c)$, does not change. There is an overall decrease in the volume occupied by the superconducting phase. The interface between the amorphous and crystalline phases becomes sharper in the process.

The interval 380 $K \leqslant T_{ann} \leqslant 430$ K is more difficult to interpret. Here a crystallization of the a-GaSb amorphous phase proper begins. The increase in the relative amount of crystalline phase, n_c, is negligible, and the changes in ρ are caused by the proximity of n_c to the percolation threshold n_c^*. In this interval of annealing temperatures, according to the structural analysis, the morphology of the samples does not undergo any substantial changes. However, there is a sharp decrease in the maximum transition temperature of the superconducting inclusions, from $T_{c1} \approx 6.5$ to $T_{c2} \approx 4.5$ K.

Significantly, this interval of annealing temperatures corresponds to $\sim (1/4 - 1/3)Q_0$, where Q_0 is the heat corresponding to the main heat-release peak on the DTA curve (Fig. 5). Since the changes in the volume fractions n_c, n_i, and n_a are small, this heat should be associated with processes which occur in the nonstoichiometric amorphous $Ga_x Sb_{1-x}$ phase (it is difficult to detect $Ga_x Sb_{1-x}$ by x-ray diffraction because its volume fraction is small). We regard a change in the short-range order of the inclusions of $Ga_x Sb_{1-x}$ phase with $x \sim 0.8$, accompanied by the evolution of latent heat of phase transition, as the most probable explanation.

The predominant process in the interval 430 $K \leqslant T_{ann} \leqslant 500$ K is crystallization of the amorphous phase. In this interval, the superconducting inclusions crystallize at a constant value $T_m = T_{c2} \approx 4.5$ K.

The precise boundaries between the various temperature intervals given above are rather arbitrary because of the scatter in the activation energies for the crystallization of the various metastable phases. As a result we find that in a-GaSb the various crystallization processes overlap; in particular, the structural changes and the changes in the volume fraction of the $Ga_x Sb_{1-x}$ phase occur over the entire temperature range studied, although their rate and nature undergo substantial changes.

The range $T_{ann} > 500$ K is characterized by an additional peak on the DTA curves and a complete suppression of superconductivity. Significantly, this heat-release peak is comparable in height to the main structural feature (Fig. 5).

According to qualitative ideas regarding the structure of the a-GaSb samples (Fig. 1) and a comparison of the DTA curves for the metallic and insulating samples (Fig. 5), one possible interpretation of the heat-release structural feature at $T_{ann} > 500$ K is a crystallization of a $Ga_x Sb_{1-x}$ phase, which is partially preserved in this interval of annealing temperatures (Fig. 7). Analysis of the superconducting properties[7] shows, however, that the relative content of superconducting inclusions is small (3–5% of the volume of the sample[5]).

If we follow this suggestion, we must therefore assume that the relative volume of superconducting inclusions with pronounced deviations from stoichiometry is very small and that most of the $Ga_x Sb_{1-x}$ phase is made up of inclusions with $x \sim 0.3$–0.4, which lie near the stoichiometric composition and which do not exhibit a superconductivity. In addition to the regions with excess gallium, we should take account of the presence of regions with excess anti-

mony (the losses of Ga and Sb in the course of the synthesis of the a-GaSb can be ignored). As a result, the substantial heat evolution may be caused by an additional contribution from inclusions with $x < 0.5$ (an excess of antimony), while only the inclusions with $x > 0.5$ are important for the superconductivity.

Along this approach, however, it is difficult to explain not only the large height but also the relative position of the additional peak on the DTA curve. Since inclusions with small deviations from stoichiometry should play a decisive role, it would be difficult to expect any significant difference between the crystallization characteristics and those of the stoichiometric amorphous a-GaSb phase. It is more likely that the crystallization temperatures of the $Ga_x Sb_{1-x}$ phase with $x \sim 0.5$ and of the amorphous a-GaSb phase are approximately equal, and we should expect the appearance of a substantially broadened, single heat-release peak. It is apparently this situation which prevails in our experiments (Figs. 5, 7, and 9), where we observe an annealing out of some of the $Ga_x Sb_{1-x}$ inclusions with $x < 0.8$ near the main heat-release peak at $T_{ann} \sim 460$ K.

Another possible interpretation of the processes which occur after the crystallization of the bulk of the tetrahedral amorphous a-GaSb phase involves recrystallization processes. The recrystallization of a polycrystalline material consists of an increase in the size of the crystalline blocks and thus a decrease in the relative volume of boundary regions in the interior of the sample.[20] A recrystallization leads to a decrease in the energy associated with boundaries; this decrease may be manifested as an exothermic peak on the DTA curves.

The recrystallization temperature T_r depends on the concentration of structural defects and/or impurities in the samples. If this concentration reaches a few tenths, the relation $T_r \approx 0.6 T_l$ becomes satisfied, where T_l is the melting point.[20] Using the values of T_l for GaSb (Fig. 1), we find the estimate $T_r \approx 580$ K, which agrees satisfactorily with the position of the additional heat-release peak (Fig. 5).

The existence of a superconductivity at $T_{ann} > 500$ K implies that the $Ga_x Sb_{1-x}$ phase is preserved at boundaries between crystallites even after the crystallization of the bulk of the metastable phases in a-GaSb. In addition, in order to explain the difference between the shape of the DTA curves for the metallic and insulating samples (Fig. 5) we must assume that the appearance of a block structure after the crystallization is a consequence of the presence of the $Ga_x Sb_{1-x}$ phase. Since the metallic sample differs from the insulating sample in having a macroscopic topological particularity (a subnetwork of conducting channels consisting of crystalline gallium antimonide and $Ga_x Sb_{1-x}$; Fig. 1), its presence could apparently determine the block structure of the crystallized a-GaSb sample.

Yet another reason for the difference between the crystallization characteristics of the $Ga_x Sb_{1-x}$ inclusions might be a size effect. It has been shown[21] that the thermodynamic properties, in particular, the stability region, may depend on both the size of a small particle and its surroundings. In the case of the melting point, for example,

the changes can reach[21] ± 40 K. In the case of disordered Ga_xSb_{1-x} inclusions of submicron size, we should apparently expect a corresponding scatter in crystallization temperature. As a result, the presence of two peaks on the DTA curve may reflect a very nonmonotonic distribution of particles with respect to size and thus respect to crystallization temperature.

It follows from this analysis that the data obtained in the present study are not an adequate basis for unambiguously resolving the nature of the processes which occur at $T_{ann} > 500$ K; the problem requires further research. The most likely explanation in our opinion is a recrystallization with a change in the stability region of the Ga_xSb_{1-x} due to a size effect.

The appearance of a disorder-induced superconductivity in the amorphous semiconductor a-GaSb was observed in Ref. 19. This effect was subsequently interpreted in Ref. 5. The interpretation was based on a nonstoichiometric amorphous Ga_xSb_{1-x} phase. In the present study we have shown that Ga_xSb_{1-x} inclusions with $x > 0.5$ make it possible to explain not only the subtle features of the superconductivity of a-GaSb (the presence of two distinct superconducting phases, corresponding to $x < 0.8$ and $x > 0.8$) but also features of the crystallization processes.

We believe that this mechanism for the onset of superconductivity (based on a local change in the short-range order) is common to a variety of semiconducting materials. In the case of gallium-containing materials, nonstoichiometric regions with an excess of gallium are responsible for the superconductivity. This opinion apparently finds support in the recent observation of superconducting anomalies in epitaxial films of gallium arsenide with a excess of arsenic.[22] In epitaxial GaAs films there are variations in the properties of the film at a scale $\sim 0.5-1$ μm due to changes in the composition of the material.[23] Since an excess of arsenic in a film does not rule out the existence of regions with a local excess of gallium, it is extremely likely that the superconductivity in GaAs arises by the same mechanism as in GaSb.

Further evidence in favor of this explanation comes from the approximate equality of the transition temperature of GaAs, $T_c \sim 10$ K, and that of amorphous gallium,[16] $T_c \sim 8-9$ K. It is not difficult to show that for gallium-rich inclusions the observed changes in the critical field H_{c1} in GaAs (Ref. 22) correspond to a Ginzburg–Landau parameter $\varkappa \sim 20$, while we have $\varkappa \sim 80$ for a-GaSb (Ref. 5). This difference can be explained in a natural way, since the degree of disorder is greater for a-GaSb; the coherence length is thus shorter than in epitaxial GaAs films. At the same time, the fairly high values of $\varkappa$ which have been suggested for GaAs indicate a significant disorder of the

epitaxial films, in accordance with the experimental situation.[23]

[1] V. I. Larchev, N. N. Mel'nik, S. V. Popova, G. G. Skrotskaya, and O. N. Talenskiĭ, Kratk. Soobshch. Fiz. FIAN SSSR, No. 1, 7 (1985).

[2] E. G. Ponyatovsky, I. T. Belash, and O. I. Barkalov, J. Non-Cryst. Solids 117–118, 679 (1990).

[3] V. F. Degtyareva, I. T. Belash, E. G. Ponyatovskiĭ, and V. I. Rasshupkin, Fiz. Tverd. Tela (Leningrad) 32, 1429 (1990) [Sov. Phys. Solid State 32, 834 (1990)].

[4] S. V. Demishev, Yu. V. Kosichkin, V. I. Larchev, A. G. Lyapin, S. V. Popova, G. G. Skrotskaya, and N. E. Sluchanko, Fiz. Tekh. Poluprovodn. 22, 1666 (1988) [Sov. Phys. Semicond. 22, 1051 (1988)].

[5] S. V. Demishev, Yu. V. Kosichkin, D. G. Lunts, A. G. Lyapin, N. E. Sluchanko, and M. S. Sharambeyan, Zh. Eksp. Teor. Fiz. 100, 707 (1991) [Sov. Phys. JETP 73, 394 (1991)].

[6] V. V. Brazhkin, S. V. Demishev, Yu. V. Kosichkin, A. G. Lyapin, N. E. Sluchanko, S. V. Frolov, and M. S. Sharambeyan, Zh. Eksp. Teor. Fiz. 101, 1908 (1992) [Sov. Phys. JETP 74, 1020 (1992)].

[7] V. V. Aleksandrova, V. D. Blank, V. I. Larchev et al., Phys. Status Solidi A 91, K5 (1985).

[8] D. S. Naidu, A. K. Sharma, D. V. K. Sastry et al., J. Non-Cryst. Solids 42, 637 (1980).

[9] V. I. Iveronova and G. P. Revkevich, Theory of x-Ray Scattering, Izd MGU, Moscow, 1978, p. 129.

[10] V. Essamet, B. Hepp, N. Proust, and J. Dixmier, J. Non-Cryst. Solids 97–98, 191 (1987).

[11] S. R. Elliott, Nature 354, 445 (1991).

[12] J. W. Christian, Theory of Transformations in Metals and Alloys, Pergamon, New York, 1975.

[13] V. V. Brazhkin, R. N. Voloshin, and S. V. Popova, J. Non-Cryst. Solids 136, 241 (1991).

[14] S. V. Demishev, Yu. V. Kosichkin, A. G. Lyapin, D. G. Dunts, and N. E. Sluchanko, Pis'ma Zh. Eksp. Teor. Fiz. 56, 44 (1992) [JETP Lett. 56, 45 (1992)].

[15] J. J. Hauser, Phys. Rev. B 11, 738 (1975).

[16] B. G. Lazarev, E. E. Semenkov, and V. I. Tutov, Vopr. At. Nauki Tekh. Ser. Fund. Prikl. Sverkhprovod., No. 1(4), 3 (1976).

[17] D. B. McWhan, G. W. Hull, T. R. R. McDonald, and E. Gregory, Science 147, 1441 (1965).

[18] R. R. McDonald, E. Gregory, and G. S. Barberich, Phys. Lett. 14, 16 (1965).

[19] S. V. Demishev, Yu. V. Kosichkin, A. G. Lyapin, and N. E. Sluchanko, Pis'ma Zh. Eksp. Teor. Fiz. 47, 654 (1988) [JETP Lett. 47, 755 (1988)].

[20] S. S. Gorelik, "Recrystallization," in Encyclopedic Dictionary of Physics, Vol. 4, Sovetskaya Entsiklopediya, Moscow, 1965, p. 408.

[21] Yu. I. Petrov, Clusters and Small Particles, Nauka, Moscow, 1986, p. 210.

[22] J. M. Baranowski, Z. M. Liliental-Weber, W.-F. Yan, and E. R. Weber, Phys. Rev. Lett. 66, 3079 (1991).

[23] A. V. Buyanov, E. P. Laurs, G. P. Peka, E. M. Semashko, and V. N. Tkachenko, Fiz. Tverd. Tela (Leningrad) 33, 2744 (1991) [Sov. Phys. Solid State 33, 1551 (1991)].

Translated by D. Parsons